CrossMark

Modeling Strength Degradation of Fiber-Reinforced Ceramic-Matrix Composites Subjected to Cyclic Loading at Elevated Temperatures in Oxidative Environments

Li Longbiao[1]

Abstract In this paper, the strength degradation of non-oxide and oxide/oxide fiber-reinforced ceramic-matrix composites (CMCs) subjected to cyclic loading at elevated temperatures in oxidative environments has been investigated. Considering damage mechanisms of matrix cracking, interface debonding, interface wear, interface oxidation and fibers fracture, the composite residual strength model has been established by combining the micro stress field of the damaged composites, the damage models, and the fracture criterion. The relationships between the composite residual strength, fatigue peak stress, interface debonding, fibers failure and cycle number have been established. The effects of peak stress level, initial and steady-state interface shear stress, fiber Weibull modulus and fiber strength, and testing temperature on the degradation of composite strength and fibers failure have been investigated. The evolution of residual strength versus cycle number curves of non-oxide and oxide/oxide CMCs under cyclic loading at elevated temperatures in oxidative environments have been predicted.

1 Introduction

Ceramic-matrix composites (CMCs) possess high strength-to-weight ratio at elevated temperatures, and are being designed in the hot section components of commercial aero engine, i.e., CFM 56 − 5B and LEAP turbofan engine (CFM International, Cincinnati, OH USA) [1]. The Civil Aviation Administration of China (CAAC) issues and enforces regulations and minimum standards covering the safe manufacture, operation and maintenance of civil aircraft. As new

✉ Li Longbiao
llb451@nuaa.edu.cn

[1] College of Civil Aviation, Nanjing University of Aeronautics and Astronautics, No.29 Yudao St, Nanjing 210016, People's Republic of China

🖄 Springer

materials, these ceramic composite components will have to meet the certification regulations of the CAAC for airworthiness. The CMC producer and user will have to show the CAAC the component is well designed for operation, safety and durability, and the failure risk is within the accepted level. However, during cyclic loading at elevated temperatures, the composite strength degrade with flight hours or cycles, which increases the failure risk level.

Under cyclic fatigue loading, the material performance of CMCs degrade with applied cycles due to damage mechanisms of matrix cracking, interface debonding, interface wear and fibers fracture. Lee et al. [2] investigated the tension − tension fatigue behavior of 2D SiC/[Si-N-C] composite at room and elevated temperatures. At room temperature, the fatigue limit was about 75% tensile strength; and at 1000 °C in air, the fatigue run-out stress level of 110 MPa was 50 MPa lower than that at room temperature, however, 35 MPa higher above the proportional limit. The area of the stress − strain loops was calculated to generate hysteresis energy density (HED) values. The fatigue hysteresis energy density decreases with applied cycles. Bertrand et al. [3] investigated the tension − tension fatigue behavior of Sylramic-iBN/BN/SiC composite at elevated temperature in a simulated combustion condition. After prior fatigue for 90,000 cycles, the tensile strength reduced by 70% under high peak stress level of 125 MPa for 1250 °C, and 35% under low peak stress level of 88 MPa for 1350 °C. The strength degradation depends not only on the test temperature but also on the applied stress level. Ruggles-Wrenn et al. [4] investigated tension − tension fatigue behavior of 2D Nextel™ 720/Alumina composite at 1200 °C in air and in steam environment under the loading frequency of 0.1 and 10 Hz. In air environment, the fatigue life appears to be independent of the loading frequency; and in steam atmosphere, the fatigue limit, number of applied cycles to failure and failure time all decrease as the loading frequency decreases, and the strength and stiffness degradation increases with decreasing frequency of prior fatigue. Mehrman et al. [5] investigated the influence of hold times on the tension − tension fatigue behavior of 2D Nextel™ 720/Alumina composite at 1200 °C in air and in steam condition. In air environment, the fatigue lives with hold times were shorter than those obtained in fatigue; and in steam atmosphere, the fatigue lives with hold times reduced significantly, and were less than those obtained in air. Ruggles-Wrenn and Lanser [6] investigated the tension − compression fatigue behavior of 2D Nextel™ 720/Alumina composite at 1200 °C in air and in steam condition. The tensile strength degraded approximately 40% after prior fatigue in steam condition, and the tension-compression cycling is much more damaging than tension − tension fatigue, due to fiber micro-buckling during compression portion of the cycle. For the non-oxide CMCs, the degradation under cyclic loading involves interface wear at room temperature, and oxidation of interphase and fibers at elevated temperature, and is accelerated by the presence of moisture. However, for the oxide/oxide CMCs, the composite is inherently resistant to oxidation at elevated temperature, but the formation of matrix cracks and degradation of fibers strength also affect the fatigue performance. Whitworth [7] evaluated the residual strength degradation in graphite/epoxy composite laminates subjected to cyclic loading, and the effects of peak stress and applied cycles on the degradation of residual strength have been analyzed. Keiji [8] developed the residual tensile strength model of fiber-reinforced CMCs after fatigue loading, and the effects of fiber strength and the interfacial shear stress on the fatigue life and residual strength of the composite have been investigated. Shah et al. [9] developed a probabilistic modeling approach to quantify the scatter in the first matrix cracking strength and the ultimate tensile strength in CMCs. Murthy et al. [10] investigated the probabilistic analysis and reliability assessment of the turbine vane withstanding a maximum temperature of 1315 °C within the substrate and the hot surface temperature of 1482 °C, considering the random variables of the material properties, strength and pressure loading on the vane. Li [11] developed approaches to

model the tensile strength of CMCs subjected to multiple fatigue loading. It was found that the loading sequence, peak stress and cycle number affect the tensile strength of the composite. Li [12] investigated the tensile strength degradation after non-stress oxidation at elevated temperature. It was found that the oxidation temperature and oxidation time affect the damage and fracture in CMCs. However, under cyclic loading at elevated temperature in oxidative environments, the composite strength significantly degrades compared with that under non-stress oxidation at elevated temperature, due to serious oxidation occurred as matrix cracks open under stress, and the wide range of interface wear/interface oxidation/fibers fracture.

The objective of this paper is to investigate the composite strength degradation of non-oxide and oxide/oxide fiber-reinforced CMCs under cyclic loading at elevated temperature in oxidative environments. Considering the damage mechanisms of matrix cracking, interface debonding, interface wear, interface oxidation and fibers fracture, the composite residual strength model has been developed by combining the micro stress field of the damaged composite, damage models and fracture criterion. The effects of peak stress level, initial and steady-state interface shear stress, fibers Weibull modulus and fibers strength, and testing temperature on the degradation of residual strength and fibers failure have been investigated. The evolution of residual strength versus cycle number curves of non-oxide and oxide/oxide CMCs under cyclic loading at elevated temperature have been predicted.

2 Residual Strength Model

Under cyclic fatigue loading, the interface shear stress and fibers strength degrade with increasing applied cycles due to the interface wear and interface oxidation [13–17]. A unit cell is extracted from the ceramic composite system to analyze the stress distributions in the fiber and the matrix, as shown in Fig. 1. The fiber radius is r_f and the matrix radius is $R(R = r_f/V_f^{1/2})$. The length of the unit cell is $l_c/2$, which is just the half matrix crack space.

When fibers break, the stress dropped by broken fibers would be transferred to intact fibers at the cross-section. The two-parameter Weibull model is adopted to describe the fibers strength distribution. The fibers fracture probability P_f is determined by Eq. (1).

$$P_f = 1 - \exp\left(-\int_{L_0} \frac{1}{l_0}\left[\frac{\sigma_f(x)}{\sigma_0}\right]^m dx\right) \quad (1)$$

where σ_0 denotes the fibers strength at the tested gauge length l_0; m denotes the fiber Weibull modulus; and L_0 denotes the integral length.
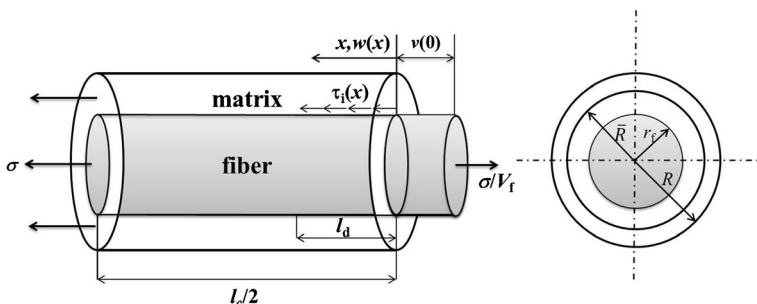

Fig. 1 The unit cell of the Budiansky-Hutchinson-Evans shear-lag model

The fracture probabilities of oxidized fibers in the oxidation region, unoxidized fibers in the oxidation region, fibers in the interface debonded region and interface bonded region of P_{fa}, P_{fb}, P_{fc} and P_{fd} are determined by Eq. (2).

$$P_{fa} = 1-\exp\left\{-2\frac{l_t}{l_0}\left[\frac{T}{\sigma_0(t)}\right]^m\right\} \tag{2}$$

$$P_{fb} = 1-\exp\left\{-2\frac{l_t}{l_0}\left(\frac{T}{\sigma_0}\right)^m\right\} \tag{3}$$

$$P_{fc} = 1-\exp\left\{-\frac{r_f T^{m+1}}{l_0(\sigma_0(N))^m \tau_i(N)(m+1)}\left[1-\left(1-\frac{l_d(N)}{l_f(N)}\right)^{m+1}\right]\right\} \tag{4}$$

$$P_{fd} = 1-\exp\left\{-\frac{2r_f T^m}{\rho l_0(\sigma_0(N))^m(m+1)\left(1-\frac{\sigma_{fo}}{T}-\frac{l_d(N)}{l_s(N)}\right)}\times\left[\left(1-\frac{l_d(N)}{l_f(N)}-\left(1-\frac{\sigma_{fo}}{T}-\frac{l_d(N)}{l_f(N)}\right)\frac{\rho l_d(N)}{r_f}\right)^{m+1}-\left(1-\frac{l_d(N)}{l_f(N)}-\left(1-\frac{\sigma_{fo}}{T}-\frac{l_d(N)}{l_f(N)}\right)\frac{\rho l_c}{2r_f}\right)^{m+1}\right]\right\} \tag{5}$$

where l_d denotes the interface debonded length; σ_{fo} denotes the fiber stress at the interface bonded region; l_f denotes the interface slip length; l_t denotes the interface oxidation region length; and $\sigma_0(t)$ denotes the time dependence of fibers strength.

$$\tau_i(N) = \tau_{io} + \left[1-\exp\left(-\omega N^\lambda\right)\right](\tau_{imin}-\tau_{io}) \tag{6}$$

$$\sigma_o(N) = \sigma_o[1-p_1(\log N)^{p_2}] \tag{7}$$

$$\sigma_0(t) = \sigma_0, t \leq \frac{1}{k}\left(\frac{K_{IC}}{Y\sigma_0}\right)^4 \tag{8}$$

$$\sigma_0(t) = \frac{K_{IC}}{Y\sqrt[4]{kt}}, t > \frac{1}{k}\left(\frac{K_{IC}}{Y\sigma_0}\right)^4 \tag{9}$$

where τ_{io} denotes the initial interface shear stress; τ_{imin} denotes the steady-state interface shear stress; ω and λ are empirical constants; p_1 and p_2 are empirical parameters; K_{IC} denotes the critical stress intensity factor; Y is a geometric parameter; and k is the parabolic rate constant.

The relationship between the applied stress, the stress carried by intact fibers and broken fibers is determined by Eq. (10).

$$\frac{\sigma}{V_f} = \left[1-P_f\left(1+\frac{2l_f}{l_c}\right)\right]T + P_r\frac{2l_f}{l_c}\langle T_b\rangle \tag{10}$$

where

$$P_f = \varphi\left[\eta P_{fa} + (1-\eta)P_{fb}\right] + P_{fc} + P_{fd} \tag{11}$$

$$P_r = P_{fc} + P_{fd} \tag{5b}$$

where η denotes the oxidation fibers fraction in the oxidized region; and φ denotes the fraction of oxidation in the multiple matrix cracks.

The stress carried by broken fibers is determined by Eq. (12).

$$\langle T_b \rangle = \frac{T}{P_r} \left(\frac{\sigma_c}{T} \right)^{m+1} \left(\frac{\sigma_o(N)}{\sigma_o} \right)^m \frac{\tau_i(N)}{\tau_i} \left\{ 1 - \exp\left[-\left(\frac{T}{\sigma_c} \right)^{m+1} \left(\frac{\sigma_o}{\sigma_o(N)} \right)^m \frac{\tau_i}{\tau_i(N)} \right] \right\} - \frac{T}{P_r} \exp\left\{ -\left(\frac{T}{\sigma_c} \right)^{m+1} \left(\frac{\sigma_o}{\sigma_o(N)} \right)^m \frac{\tau_i}{\tau_i(N)} \right\} \quad (12)$$

Substituting Eqs. (2), (8), (11) and (12) into the Eq. (10), the composite residual strength can be determined subjected to cyclic loading at elevated temperature in oxidative environments considering interface wear, interface oxidation, fibers oxidation and fracture.

3 Discussions

The ceramic composite system of SiC/SiC is used for the case study and its basic material properties are given by [18]: $V_f = 30\%$, $E_f = 230$ GPa, $E_m = 350$ GPa, $r_f = 7.5$ μm, $m = 3$, $l_0 = 25 \times 10^{-3}$ m and $\sigma_0 = 0.5$ GPa; the interface shear stress degradation model parameters are given by: $\tau_{io} = 50$ MPa, $\tau_{imin} = 1.0$ MPa, $\omega = 0.0001$ and $\lambda = 1.2$; and the fiber strength degradation model parameters are given by: $p_1 = 0.02$ and $p_2 = 1.4$. The effects of fatigue peak stress level, interface shear stress, fiber Weibull modulus, fibers strength and testing temperature on the composite strength degradation versus applied cycles have been analyzed.

3.1 Effect of Peak Stress Level

The effects of peak stress level, i.e., $\sigma_{max} = 180$ and 200 MPa, on the evolution of residual strength versus applied cycles, and the fibers failure versus applied stress are illustrated in Fig. 2.

When $\sigma_{max} = 180$ MPa, the composite residual strength decreases with increasing applied cycles, i.e., 364, 343, 314 and 194 MPa corresponding to the cycle number of $N = 1$, 100, 1000 and 3000, as shown in Fig. 2a; and the broken fibers fraction versus applied stress curves after experiencing 1, 100, 1000 and 3000 applied cycles under $\sigma_{max} = 180$ MPa are illustrated in Fig. 2b, in which the residual strength decreases with increasing cycle number.

When $\sigma_{max} = 200$ MPa, the composite residual strength decreases with increasing applied cycles, i.e., 364, 338, 310 and 166 MPa corresponding to the cycle number of $N = 1$, 100, 1000 and 3000, as shown in Fig. 2a; and the broken fibers fraction versus applied stress curves after experiencing 1, 100, 1000 and 3000 applied cycles under $\sigma_{max} = 200$ MPa are illustrated in Fig. 2c, in which the residual strength decreases with increasing cycle number.

With increasing peak stress level, the composite residual strength degrades due to the increasing interface wear and interface debonded region.

3.2 Effect of Interface Shear Stress

The effects of interface shear stress, i.e., $\tau_i = 20$ and 40 MPa, on the evolution of composite residual strength versus applied cycles, and the broken fibers fraction versus applied stress after experiencing cyclic loading at $\sigma_{max} = 180$ MPa are illustrated in Fig. 3.
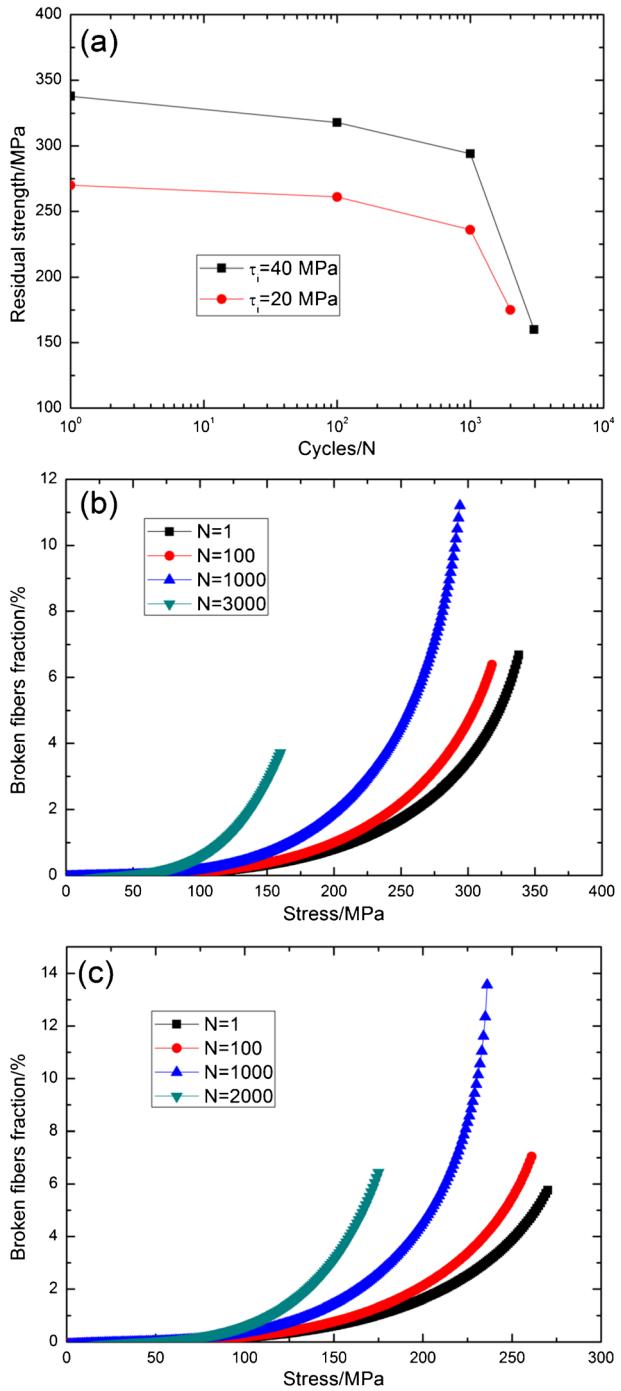
When $\tau_i = 40$ MPa, the composite residual strength decreases with increasing applied cycles, i.e., 338, 318, 294 and 160 MPa corresponding to the cycle number of $N = 1$, 100, 1000 and

Fig. 2 a The residual strength versus cycle number curves under σ_{max} = 180 and 200 MPa; **b** the broken fibers fraction versus applied stress curves after experiencing different applied cycles under σ_{max} = 180 MPa; and **c** the broken fibers fraction versus applied stress curves after experiencing different applied cycles under σ_{max} = 200 MPa
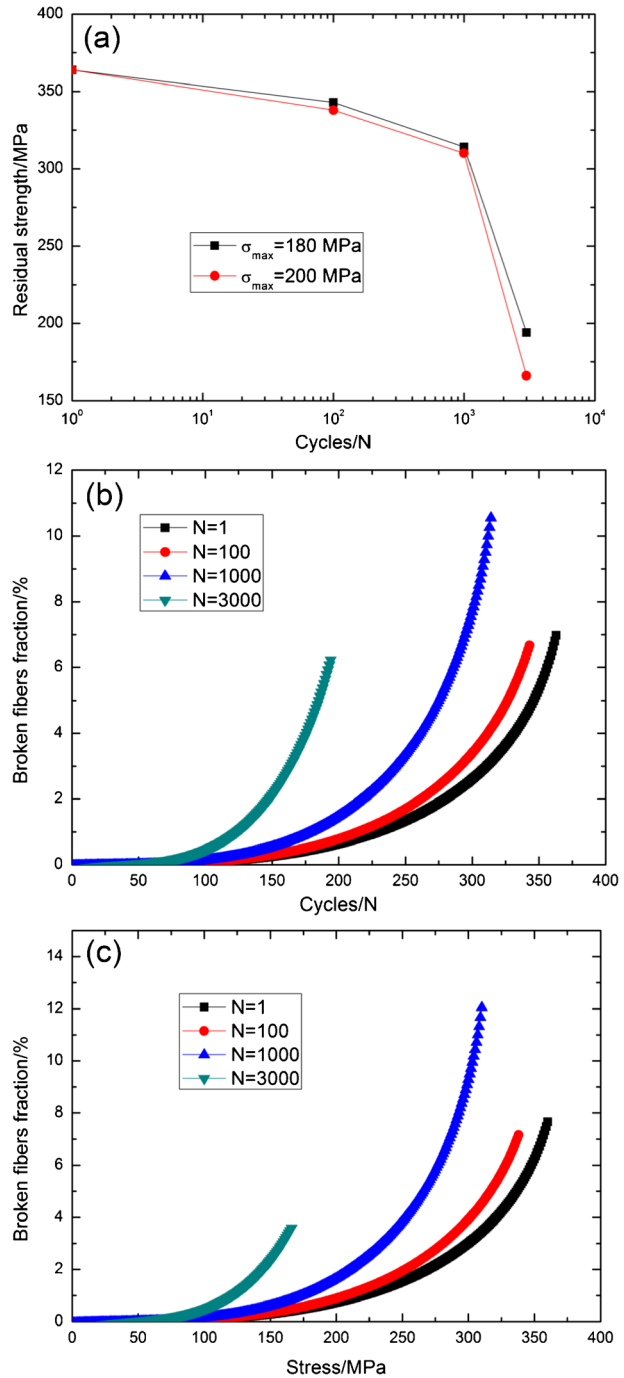
3000 at σ_{max} = 180 MPa, as shown in Fig. 3a; and the broken fibers fraction versus applied stress curves after experiencing 1, 100, 1000 and 3000 applied cycles under σ_{max} = 180 MPa are illustrated in Fig. 3b, in which the residual strength decreases with increasing cycle number.

Fig. 3 a The residual strength versus cycle number curves corresponding to $\tau_i = 20$ and 40 MPa under $\sigma_{max} = 180$ MPa; b the broken fibers fraction versus applied stress curves after experiencing different applied cycles corresponding to $\tau_i = 40$ MPa under $\sigma_{max} = 180$ MPa; and c the broken fibers fraction versus applied stress curves after experiencing different applied cycles corresponding to $\tau_i = 20$ MPa under $\sigma_{max} = 180$ MPa

When $\tau_i = 20$ MPa, the composite residual strength decreases with increasing applied cycles, i.e., 270, 261, 236 and 175 MPa corresponding to the cycle number of $N = 1, 100, 1000$

and 3000 at $\sigma_{max} = 180$ MPa, as shown in Fig. 3a; and the broken fibers fraction versus applied stress curves after experiencing 1, 100, 1000 and 3000 applied cycles under $\sigma_{max} = 180$ MPa are illustrated in Fig. 3c, in which the residual strength decreases with increasing cycle number.

The effects of interface shear stress, i.e., $\tau_f = 5$ and 10 MPa, on the evolution of composite residual strength versus applied cycles, and the broken fibers fraction versus applied stress after experiencing cyclic loading at $\sigma_{max} = 180$ MPa are illustrated in Fig. 4.

When $\tau_f = 10$ MPa, the composite residual strength decreases with increasing applied cycles, i.e., 292, 277, 259 and 228 MPa corresponding to the cycle number of $N = 1$, 100, 1000 and 3000 at $\sigma_{max} = 180$ MPa, as shown in Fig. 4a; and the broken fibers fraction versus applied stress curves after experiencing 1, 100, 1000 and 3000 applied cycles under $\sigma_{max} = 180$ MPa are illustrated in Fig. 4b, in which the residual strength decreases with increasing cycle number.

When $\tau_f = 5$ MPa, the composite residual strength decreases with increasing applied cycles, i.e., 292, 276, 256 and 198 MPa corresponding to the cycle number of $N = 1$, 100, 1000 and 3000 at $\sigma_{max} = 180$ MPa, as shown in Fig. 4a; and the broken fibers fraction versus applied stress curves after experiencing 1, 100, 1000 and 3000 applied cycles under $\sigma_{max} = 180$ MPa are illustrated in Fig. 4c, in which the residual strength decreases with increasing cycle number.

With increasing of initial and steady-state interface shear stress, the composite residual strength increases due to the decrease of the interface wear and interface debonding range.

3.3 Effect of Fiber Weibull Modulus

The effects of fiber Weibull modulus, i.e., $m = 3$ and 5, on the evolution of composite residual strength versus applied cycles, and the broken fibers fraction versus applied stress after experiencing cyclic loading at $\sigma_{max} = 180$ MPa are illustrated in Fig. 5.

When $m = 3$, the composite residual strength decreases with increasing applied cycles, i.e., 360, 338, 310 and 166 MPa corresponding to the cycle number of $N = 1$, 100, 1000 and 3000 at $\sigma_{max} = 180$ MPa, as shown in Fig. 5a; and the broken fibers fraction versus applied stress curves after experiencing 1, 100, 1000 and 3000 applied cycles under $\sigma_{max} = 180$ MPa are illustrated in Fig. 5b, in which the composite residual strength decreases with increasing cycle number.
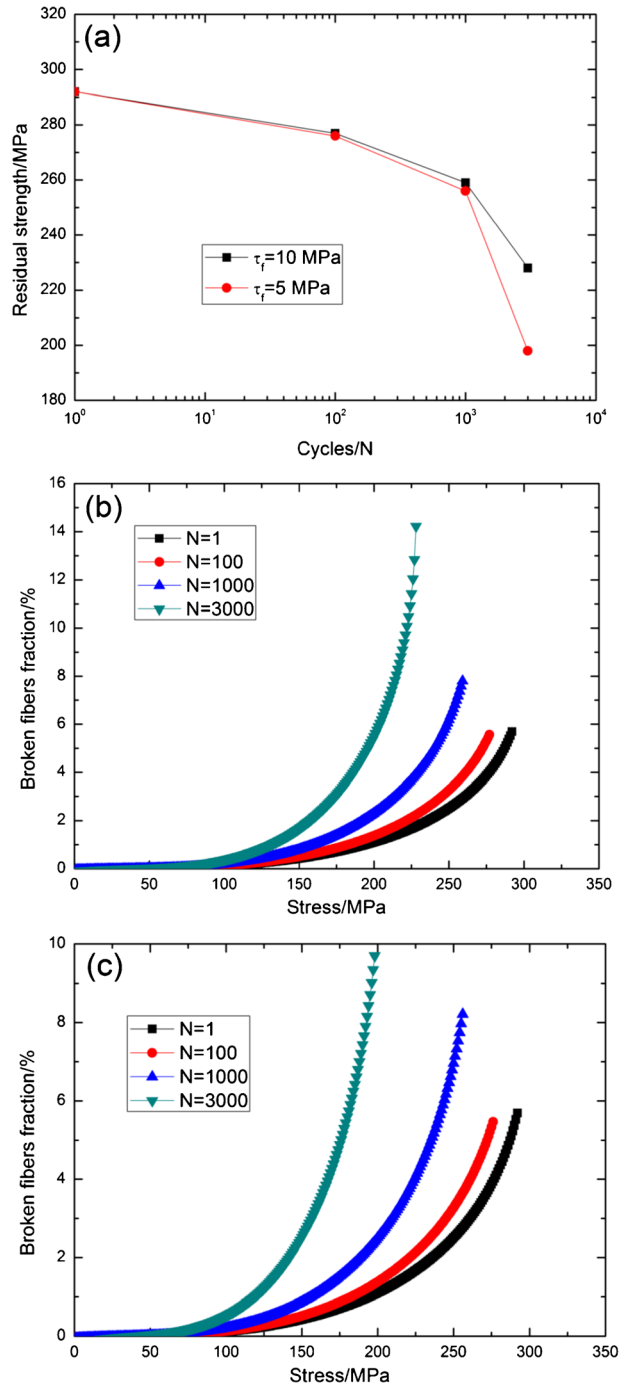
When $m = 5$, the composite residual strength decreases with increasing applied cycles, i.e., 242, 230, 202 and 147 MPa corresponding to the cycle number of $N = 1$, 100, 1000 and 3000 at $\sigma_{max} = 180$ MPa, as shown in Fig. 5a; and the broken fibers fraction versus applied stress curves after experiencing 1, 100, 1000 and 3000 applied cycles under $\sigma_{max} = 180$ MPa are illustrated in Fig. 5c, in which the composite residual strength decreases with increasing cycle number.

With increasing of fiber Weibull modulus, the composite residual strength after experiencing cyclic loading decreases.

3.4 Effect of Fiber Strength

The effects of fiber strength, i.e., $\sigma_0 = 0.3$ and 0.5 GPa, on the evolution of composite residual strength versus applied cycles, and the broken fibers fraction versus applied stress after experiencing cyclic loading at $\sigma_{max} = 180$ MPa are illustrated in Fig. 6.
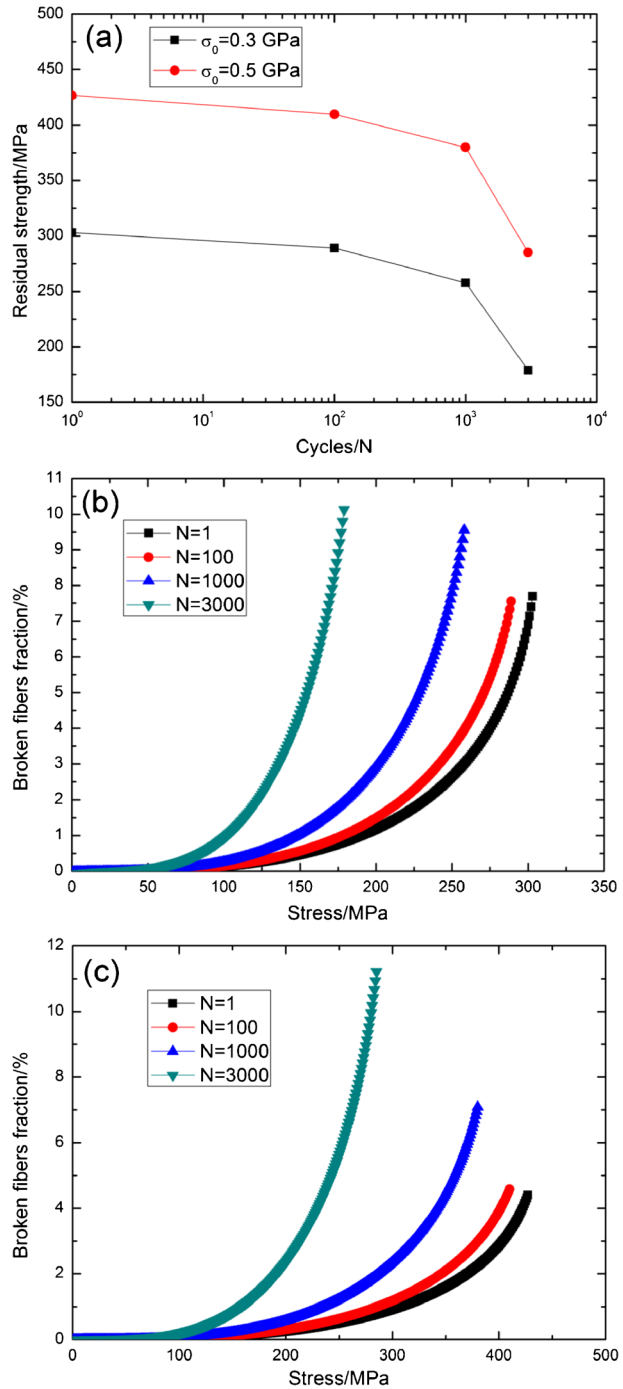
When $\sigma_0 = 0.3$ GPa, the composite residual strength decreases with increasing applied cycles, i.e., 303, 289, 258 and 179 MPa corresponding to the cycle number of $N = 1$, 100, 1000 and 3000 at $\sigma_{max} = 180$ MPa, as shown in Fig. 6a; and the broken fibers fraction versus applied stress curves after experiencing 1, 100, 1000 and 3000 applied cycles under $\sigma_{max} = 180$ MPa are illustrated in Fig. 6b, in which the residual strength decreases with increasing cycle number.

Fig. 4 a The residual strength versus cycle number curves corresponding to τ_f = 5 and 10 MPa under σ_{max} = 180 MPa; **b** the broken fibers fraction versus applied stress curves after experiencing different applied cycles corresponding to τ_f = 10 MPa under σ_{max} = 180 MPa; and **c** the broken fibers fraction versus applied stress curves after experiencing different applied cycles corresponding to τ_f = 5 MPa under σ_{max} = 180 MPa

When σ_0 = 0.5 GPa, the composite residual strength decreases with increasing applied cycles, i.e., 427, 410, 380 and 285 MPa corresponding to the cycle number of N = 1, 100, 1000 and 3000 at σ_{max} = 180 MPa, as shown in Fig. 6a; and the broken fibers fraction versus applied

Fig. 5 **a** The residual strength versus cycle number curves corresponding to $m = 3$ and 5 under $\sigma_{max} = 180$ MPa; **b** the broken fibers fraction versus applied stress curves after experiencing different applied cycles corresponding to $m = 3$ under $\sigma_{max} = 180$ MPa; and **c** the broken fibers fraction versus applied stress curves after experiencing different applied cycles corresponding to $m = 5$ under $\sigma_{max} = 180$ MPa
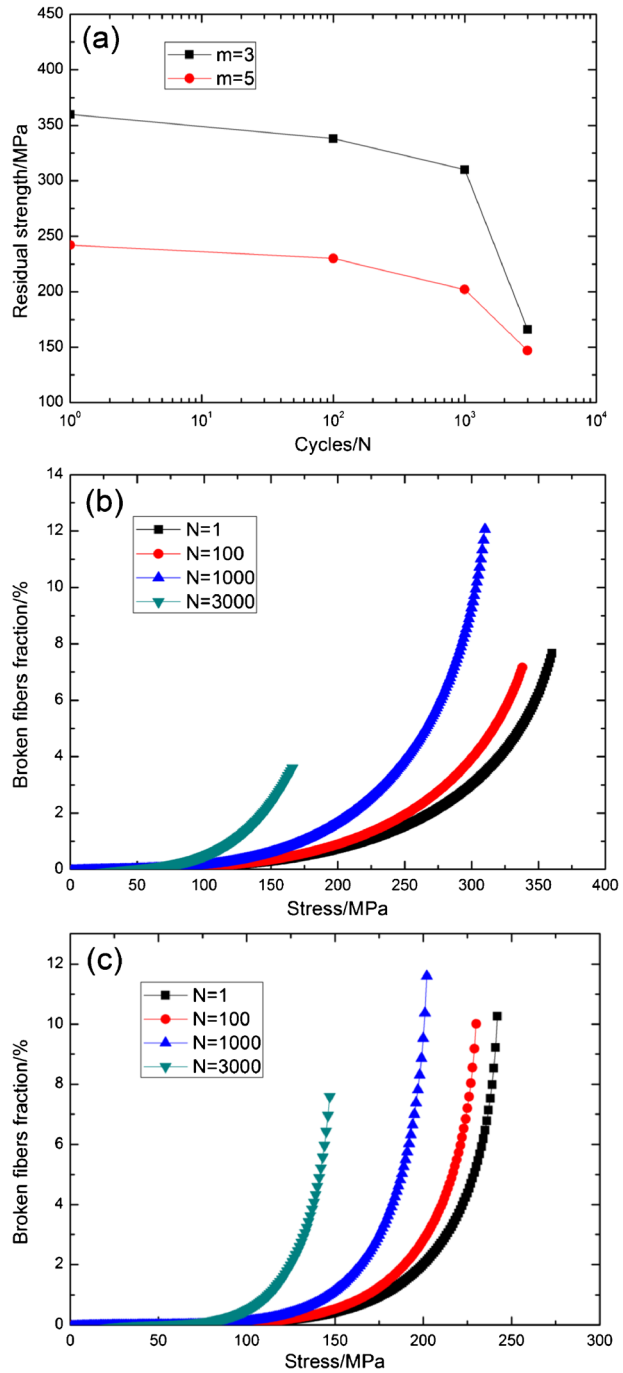
stress curves after experiencing 1, 100, 1000 and 3000 applied cycles under $\sigma_{max} = 180$ MPa are illustrated in Fig. 6c, in which the residual strength decreases with increasing cycle number.

Fig. 6 **a** The residual strength versus cycle number curves corresponding to $\sigma_0 = 0.3$ and 0.5 GPa under $\sigma_{max} = 180$ MPa; **b** the broken fibers fraction versus applied stress curves after experiencing different applied cycles corresponding to $\sigma_0 = 0.3$ GPa under $\sigma_{max} = 180$ MPa; and **c** the broken fibers fraction versus applied stress curves after experiencing different applied cycles corresponding to $\sigma_0 = 0.5$ GPa under $\sigma_{max} = 180$ MPa

With increasing of fibers strength, the composite residual strength after experiencing cyclic loading increases.

Fig. 7 **a** The residual strength versus cycle number curves corresponding to Tem = 600 °C and 800 °C under σ_{max} = 180 MPa; **b** the broken fibers fraction versus applied stress curves after experiencing different applied cycles 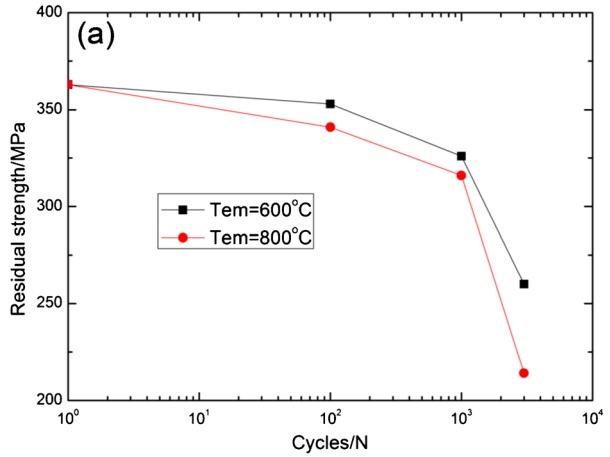corresponding to Tem = 600 °C under σ_{max} = 180 MPa; and **c** the broken fibers fraction versus applied stress curves after experiencing different applied cycles corresponding to Tem = 800 °C under σ_{max} = 180 MPa
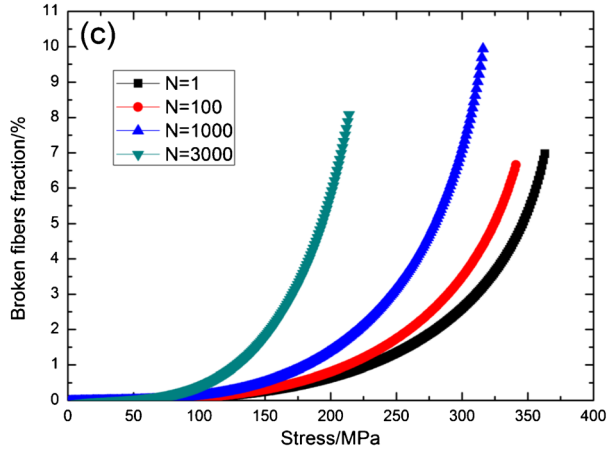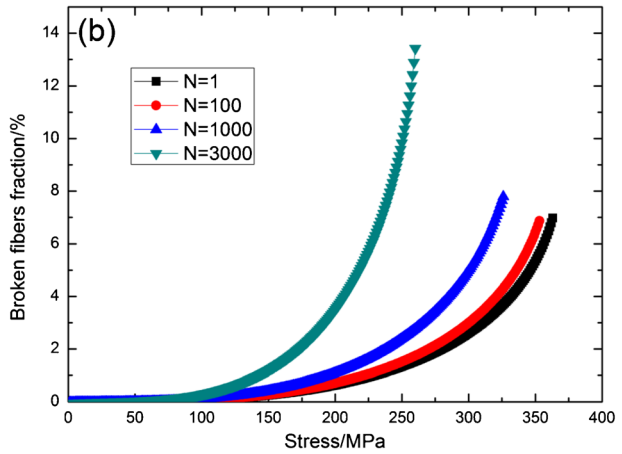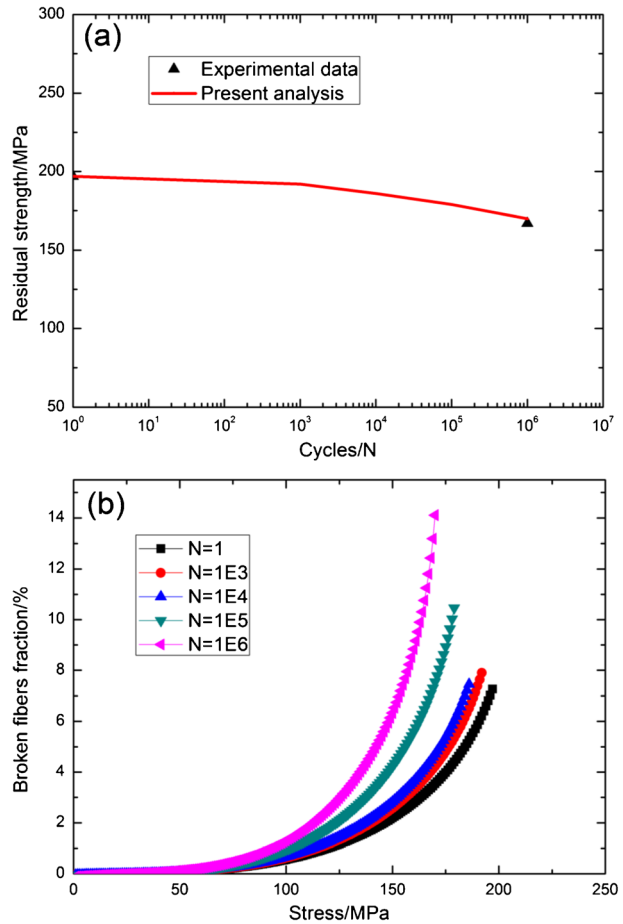
3.5 Effect of Testing Temperatures

The effects of testing temperature, i.e., Tem = 600 °C and 800 °C, on the evolution of composite residual strength versus applied cycles, and the broken fibers fraction versus applied stress after experiencing cyclic loading at $\sigma_{max} = 180$ MPa are illustrated in Fig. 7.

When Tem = 600 °C, the composite residual strength decreases with increasing applied cycles, i.e., 363, 353, 326 and 260 MPa corresponding to the cycle number of $N = 1$, 100, 1000 and 3000 at $\sigma_{max} = 180$ MPa, as shown in Fig. 7a; and the broken fibers fraction versus applied stress curves after experiencing 1, 100, 1000 and 3000 applied cycles under $\sigma_{max} = 180$ MPa are illustrated in Fig. 7b, in which the residual strength decreases with increasing cycle number.
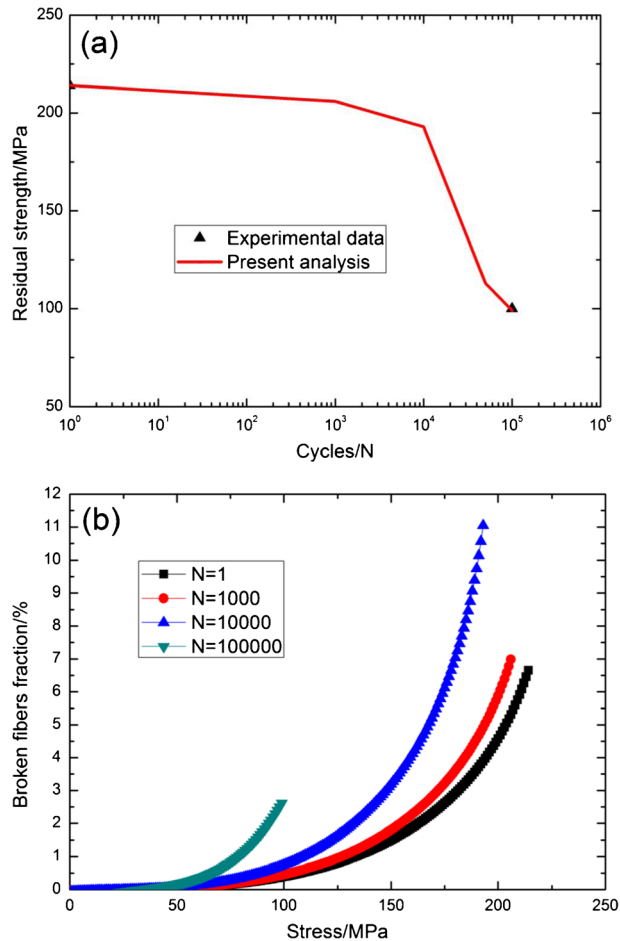
When Tem = 800 °C, the composite residual strength decreases with increasing applied cycles, i.e., 363, 341, 316 and 214 MPa corresponding to the cycle number of $N = 1$, 100, 1000 and 3000 at $\sigma_{max} = 180$ MPa, as shown in Fig. 7a; and the broken fibers fraction versus applied stress curves after experiencing 1, 100, 1000 and 3000 applied cycles under $\sigma_{max} = 180$ MPa are illustrated in Fig. 7c, in which the residual strength decreases with increasing cycle number.

With increasing of testing temperature, the composite residual strength after experiencing cyclic loading decreases.

4 Experimental Comparisons

4.1 Non-oxide CMCs

Lee et al. [2] investigated the tension − tension fatigue behavior of SiC/Si-N-C composite at room temperature and 1000 °C. At room temperature, the composite tensile strength was about 197 MPa, after experiencing 1,000,000 applied cycles under the fatigue peak stress of 125 MPa, the tensile strength degrades to approximately 167 MPa, and the strength decreases about 15%. The experimental and theoretical predicted composite residual strength versus applied cycles curves are illustrated in Fig. 8a. The residual strength decreases with increasing applied cycles, i.e., 197, 192, 186, 179 and 170 MPa corresponding to the cycle number of $N = 1$, 1000, 10,000, 100,000 and 1,000,000 at $\sigma_{max} = 125$ MPa. The broken fibers fraction versus applied stress curves after experiencing 1, 1000, 10,000, 100,000 and 1,000,000 applied cycles under $\sigma_{max} = 125$ MPa are illustrated in Fig. 8b. At 1000 °C, the composite tensile strength was about 214 MPa, after experiencing 100,000 under the fatigue peak stress of 100 MPa, the tensile strength degrades to approximately 157 MPa, and the strength decreases about 26%. The experimental and theoretical
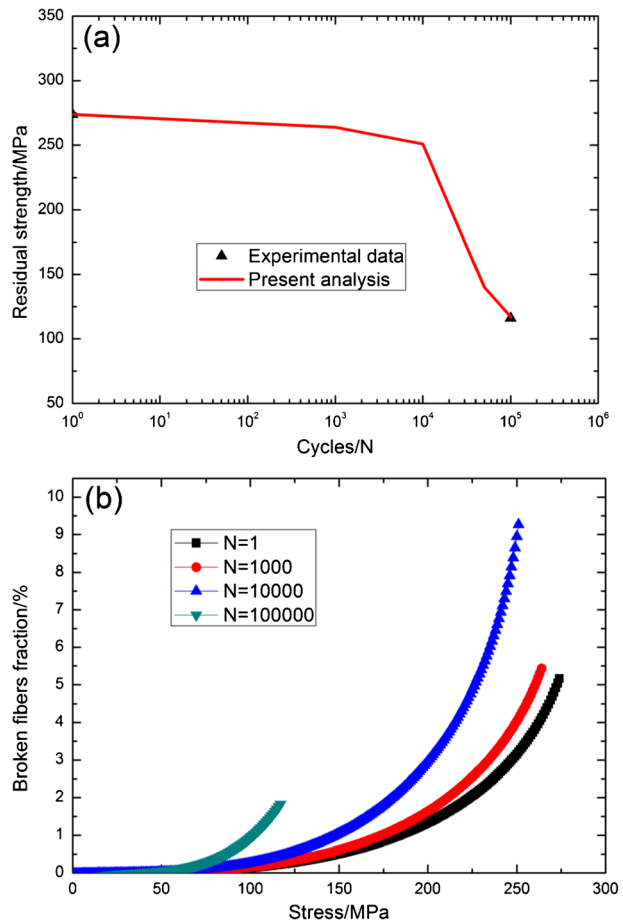
Fig. 9 **a** The residual strength versus applied cycles; and **b** the broken fibers versus applied cycles of SiC/Si-N-C composites under fatigue peak stress of $\sigma_{max} = 100$ MPa at 1000 °C

predicted composite residual strength versus applied cycles curves are illustrated in Fig. 9a. The residual strength decreases with increasing applied cycles, i.e., 214, 206, 193, 113 and 99 MPa corresponding to the cycle number of $N = 1$, 1000, 10,000, 50,000 and 100,000 at $\sigma_{max} = 100$ MPa. The broken fibers fraction versus applied stress curves after experiencing 1, 1000, 10,000 and 100,000 applied cycles under $\sigma_{max} = 100$ MPa are illustrated in Fig. 9b.

Bertrand et al. [3] investigated the tension − tension fatigue behavior of SiC/SiC composite at 1250 °C and 1350 °C. The composite tensile strength was about 274 MPa at elevated temperature. At 1250 °C, the composite residual strength decreases to 116 MPa after experiencing 100,000 applied cycles under the fatigue peak stress of 125 MPa, and the composite strength degrades approximately 57%. The experimental and theoretical predicted composite residual strength versus applied cycles curves are illustrated in Fig. 10a. The residual strength decreases with increasing applied cycles, i.e., 274, 264, 251, 140 and 117 MPa corresponding to the cycle number of $N = 1$, 1000, 10,000, 50,000 and 100,000 at $\sigma_{max} = 125$ MPa. The broken fibers fraction versus applied stress curves after experiencing 1, 1000, 10,000 and 100,000 applied cycles under $\sigma_{max} = 125$ MPa are illustrated in Fig. 10b. At 1350 °C, the composite residual strength decreases to 247 MPa after experiencing 100,000

Fig. 10 a The residual strength versus applied cycles; and b the broken fibers versus applied cycles of SiC/Si-N-C composites under fatigue peak stress of $\sigma_{max} = 125$ MPa at 1250 °C
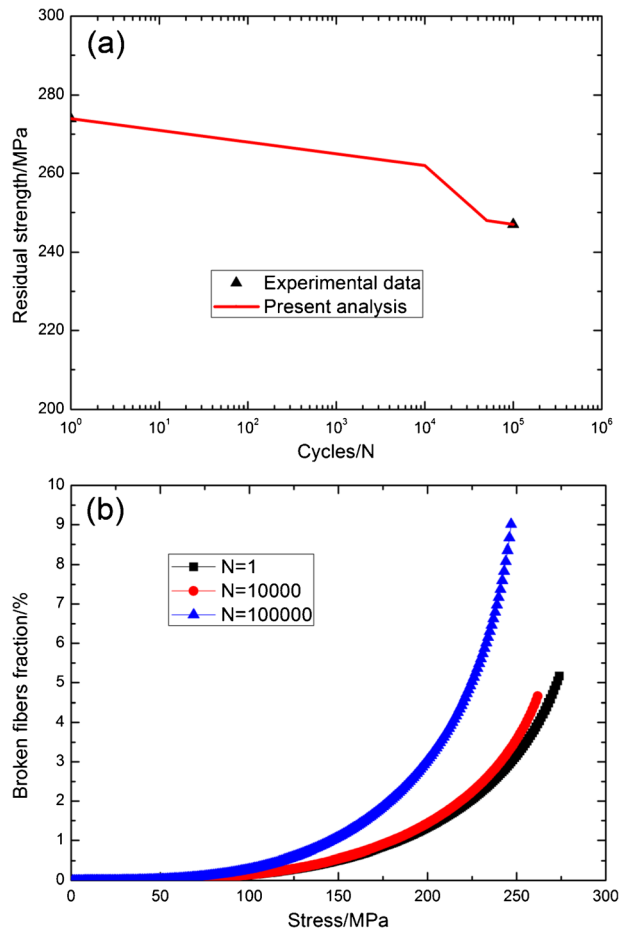
applied cycles under the fatigue peak stress of 90 MPa, and the composite strength degrades approximately 10%. The experimental and theoretical predicted composite residual strength versus applied cycles curves are illustrated in Fig. 11a. The residual strength decreases with increasing applied cycles, i.e., 274, 262, 248, and 247 MPa corresponding to the cycle number of $N = 1$, 10,000, 50,000 and 100,000 at $\sigma_{max} = 90$ MPa. The broken fibers fraction versus applied stress curves after experiencing 1, 10,000 and 100,000 applied cycles under $\sigma_{max} = 90$ MPa are illustrated in Fig. 11b.

4.2 Oxide/Oxide CMCs

Ruggles-Wrenn et al. [4] investigated the tension − tension fatigue behavior of 2D Nextel™ 720/Alumina composite under the loading frequency of 1.0 Hz at 1200 °C in steam atmosphere. The ultimate tensile strength was 190 MPa. Under the fatigue peak stress of 100 MPa, the composite residual strength decreases to 174 MPa after experiencing 100,000 applied cycles, and the composite strength degrades approximately 8.4%; and under the fatigue peak stress of 125 MPa, the composite residual strength decreases to 168 MPa after experiencing

Fig. 11 a The residual strength versus applied cycles; and b the broken fibers versus applied cycles of SiC/Si-N-C composites under fatigue peak stress of $\sigma_{max} = 90$ MPa at 1350 °C

100,000 applied cycles, and the composite strength degrades approximately 11.5%. The experimental and theoretical predicted composite residual strength versus applied cycles curves under σ_{max} = 100 MPa are illustrated in Fig. 12a. The residual strength decreases with increasing applied cycles, i.e., 190, 188, 185 and 173 MPa corresponding to the cycle number of N = 1, 1000, 10,000 and 100,000 at σ_{max} = 100 MPa. The broken fibers fraction versus applied stress curves after experiencing 1, 1000, 10,000 and 100,000 applied cycles under σ_{max} = 100 MPa are illustrated in Fig. 12b. The experimental and theoretical predicted composite residual strength versus applied cycles curves under σ_{max} = 125 MPa are illustrated in Fig. 13a. The residual strength decreases with increasing applied cycles, i.e., 190, 183, 182 and 167 MPa corresponding to the cycle number of N = 1, 1000, 10,000 and 100,000 at σ_{max} = 125 MPa. The broken fibers fraction versus applied stress curves after experiencing 1, 1000, 10,000 and 100,000 applied cycles under σ_{max} = 125 MPa are illustrated in Fig. 13b.

4.3 Conclusions

In this paper, the strength degradation of non-oxide and oxide/oxide fiber-reinforced ceramic-matrix composites (CMCs) subjected to cyclic loading at elevated temperature in oxidative


Fig. 12 **a** The residual strength versus applied cycles; and **b** the broken fibers versus applied cycles of Nextel™ 720/Alumina composites under fatigue peak stress of σ_{max} = 100 MPa at 1200 °C
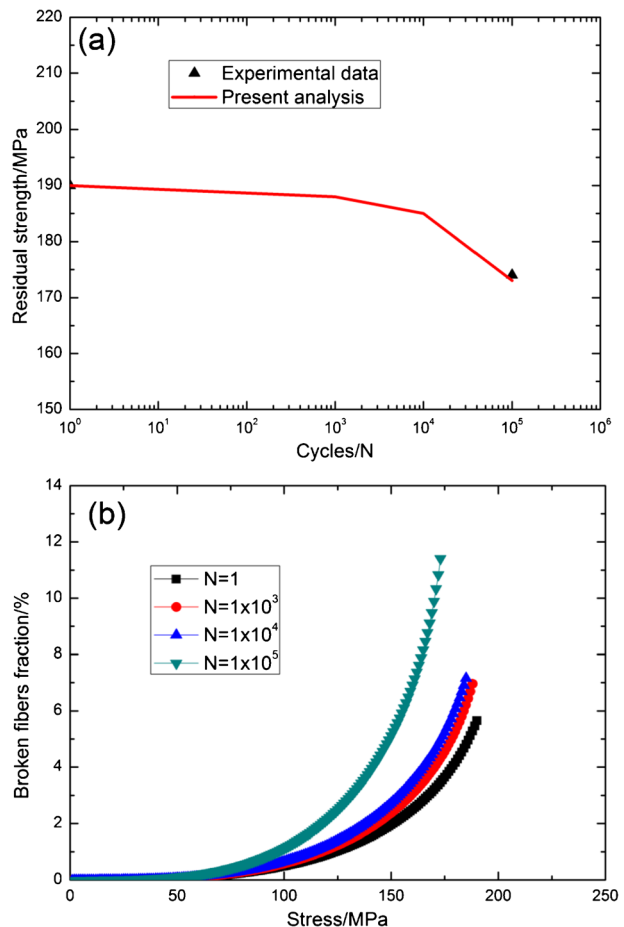
environments has been investigated. Considering the damage mechanisms of matrix cracking, interface debonding, interface wear, interface oxidation and fibers fracture, the composite residual strength model has been established by combining the micro stress field of the damaged composites, the damage models and the fracture criterion. The effects of peak stress level, initial and steady-state interface shear stress, fiber Weibull modulus and fibers strength, and testing temperature on the degradation of composite strength and fibers failure have been investigated. The evolution of residual strength versus cycle number curves of SiC/Si-N-C, SiC/SiC and Nextel™ 720/Alumina composites under cyclic loading at elevated temperatures in oxidative environments have been predicted.

(1) With increasing of peak stress level, the composite residual strength after experiencing cyclic loading decreases, due to the increasing range of interface debonding and interface wear.

(2) With increasing of initial and steady-state interface shear stress, the composite residual strength after experiencing cyclic loading increases, due to the decrease of interface debonding and interface wear range.

(3) With increasing of fiber Weibull modulus, the composite residual strength after experiencing cyclic loading decreases.

Fig. 13 **a** The residual strength versus applied cycles; and **b** the broken fibers versus applied cycles of Nextel™ 720/Alumina composites under fatigue peak stress of $\sigma_{max} = 125$ MPa at 1200 °C
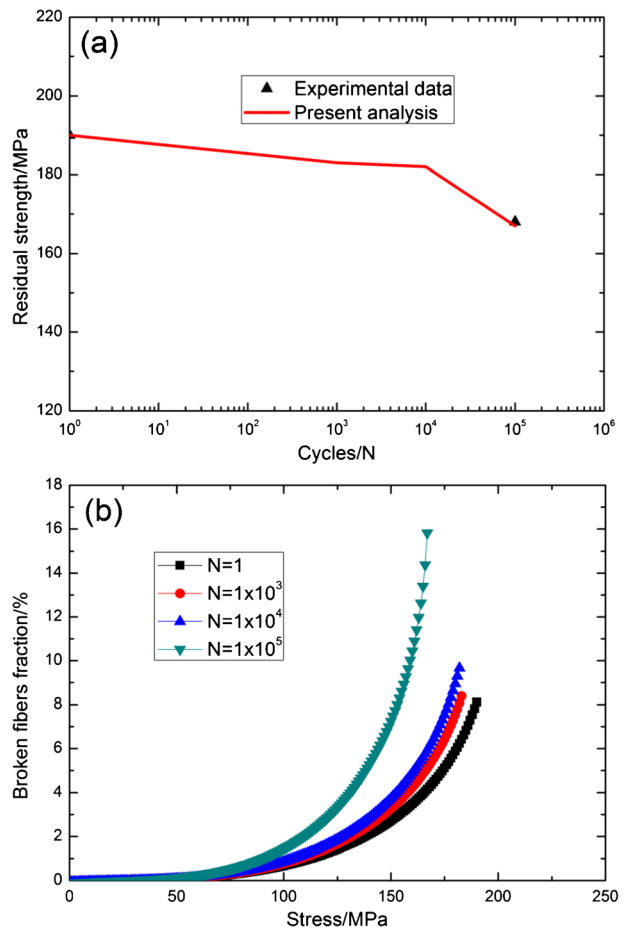
(4) With increasing of fiber strength, the composite residual strength after experiencing cyclic loading increases.

(5) With increasing of testing temperature, the composite residual strength after experiencing cyclic loading decreases due to the interface oxidation and fibers strength degradation.

References

1. Gonczy, S.T.: Federal Aviation Administration (FAA) airworthiness certification for ceramic matrix composite components in civil aircraft systems. MATEC Web of Conferences. **29**, 00002 (2015). doi:10.1051/matecconf/20152900002
2. Lee, S.S., Zawada, L.P., Staehler, J.M., Folsom, G.A.: Mechanical behavior and high-temperature performance of a woven Nicalon™/Si-N-C ceramic-matrix composite. J. Am. Ceram. Soc. **81**, 1797–1811 (1998). doi:10.1111/j.1151-2916.1998.tb02550.x
3. Bertrand, D.J., Sabelkin, V., Zawada, L., Mall, S.: Fatigue behavior of Sylramic-iBN/BN/CVI SiC ceramic matrix composite in combustion environment. J. Mater. Sci. **50**, 7437–7447 (2015). doi:10.1007/s10853-015-9302-8
4. Ruggles-Wrenn, M.B., Hetrick, G., Baek, S.S.: Effects of frequency and environment on fatigue behavior of an oxide-oxide ceramic composite at 1200°C. Int. J. Fatigue. **30**, 502–516 (2008). doi:10.1016/j.ijfatigue.2007.04.004
5. Mehrman, J.M., Ruggles-Wrenn, M.B., Baek, S.S.: Influence of hold times on the elevated-temperature fatigue behavior of an oxide-oxide ceramic composite in air and in steam environment. Compos. Sci. Technol. **67**, 1425–1438 (2007). doi:10.1016/j.compscitech.2006.09.005
6. Ruggles-Wrenn, M.B., Lanser, R.L.: Tension-compression fatigue of an oxide/oxide ceramic composite at elevated temperature. Mater. Sci. Eng. A. **659**, 270–277 (2016). doi:10.1016/j.msea.2016.02.057
7. Whitworth, H.A.: Evaluation of the residual strength degradation in composite laminates under fatigue loading. Compos. Struct. **48**, 261–264 (2000). doi:10.1016/S0263-8223(99)00113-0
8. Keiji, O.: Prediction of residual tensile strength after fatigue in unidirectional brittle fiber-reinforced ceramic composites. J. Solid Mech. Mater. Eng. **5**, 64–74 (2011). doi:10.1299/jmmp.5.64
9. Shah, A.R., Murthy, P.L.N., Mital, S.K., Bhatt, R.T.: Probabilistic modeling of ceramic matrix composite strength. J. Compos. Mater. **34**, 670–688 (2000). doi:10.1177/002199830003400803
10. Murthy, P.L.N., Nemeth, N.N., Brewer, D.N., Mital, S.: Probabilistic analysis of a SiC/SiC ceramic matrix composite turbine vane. Composites Part B. **39**, 694–703 (2008). doi:10.1016/j.compositesb.2007.05.006
11. Li, L.B.: Modeling the tensile strength of carbon fiber-reinforced ceramic-matrix composites under multiple fatigue loading. Appl. Compos. Mater. **23**, 313–336 (2016). doi:10.1007/s10443-015-9462-3
12. Li, L.B.: Modeling the effect of oxidation on tensile strength of carbon fiber-reinforced ceramic-matrix composites. Appl. Compos. Mater. **22**, 921–943 (2015). doi:10.1007/s10443-015-9443-6
13. Holmes, J.W.: Influence of stress ratio on the elevated-temperature fatigue of a silicon carbide fiber-reinforced silicon nitride composite. J. Am. Ceram. Soc. **74**, 1639–1645 (1991). doi:10.1111/j.1151-2916.1991.tb07152.x
14. McNulty, J.C., Zok, F.W.: Low-cycle fatigue of Nicalon-fiber-reinforced ceramic composites. Compos. Sci. Technol. **59**, 1597–1607 (1999). doi:10.1016/S0266-3538(99)00019-6
15. Li, L.B.: Assessment of the interfacial properties from fatigue hysteresis loss energy in ceramic-matrix composites with different fiber preforms at room and elevated temperatures. Mater. Sci. Eng. A. **613**, 17–36 (2014). doi:10.1016/j.msea.2014.06.092
16. Fantozzi, G., Reynaud, P.: Mechanical behavior of SiC fiber-reinforced ceramic matrix composites. Comprehensive Hard Materials. 345–366 (2014). doi:10.1016/B978–0–08-096527-7.00031-3
17. Ruggles-Wrenn, M.B., Lee, M.D.: Fatigue behavior of an advanced SiC/SiC ceramic composite with a self-healing matrix at 1300°C in air and in steam. Mater. Sci. Eng. A. **677**, 438–445 (2016). doi:10.1016/j.msea.2016.09.076
18. Li, L.B.: Damage development in fiber-reinforced ceramic-matrix composites under cyclic fatigue loading using hysteresis loops at room and elevated temperatures. Int. J. Fract. **199**, 39–58 (2016). doi:10.1007/s10704-016-0085-y